UDK 669.35:621.785:620.181
Professional article/Strokovni članek

ISSN 1580-2949
MTAEC9, 48(4)599(2014)

INFLUENCE OF HEAT TREATMENT ON THE MICROSTRUCTURE AND MECHANICAL PROPERTIES OF ALUMINIUM BRONZE

VPLIV TOPLOTNE OBDELAVE NA MIKROSTRUKTURO IN MEHANSKE LASTNOSTI ALUMINIJEVEGA BRONA

Peter Sláma, Jaromír Dlouhý, Michal Kövér

COMTES FHT a.s., Prumyslova 995, 334 41 Dobrany, Czech Republic
peter.slama@comtesfht.cz

Prejem rokopisa – received: 2013-10-03; sprejem za objavo – accepted for publication: 2013-10-24

The paper deals with the influence of heat treatment (annealing, quenching and aging) on the microstructure and mechanical properties of pressed bars made from the CuAl10Ni5Fe4 alloy. The microstructures were observed in light and scanning electron microscopes. The appearance and area fractions of the α and κ phases and their influence on the mechanical properties were examined. Using DSC and EBSD methods, the presence of the γ_2 phase was monitored, as it is a very hard and brittle phase that impairs the material's corrosion resistance. The results were compared with data for the high-alloyed CuAl14Fe5 aluminium bronze, in which high hardness and wear resistance are imparted by the $\beta + \gamma_2$ phases.

Keywords: aluminium bronze, heat treatment, microstructure, mechanical properties, DSC, EBSD, γ_2-phase

Članek obravnava vpliv toplotne obdelave (žarjenje, kaljenje in staranje) na mikrostrukturo in mehanske lastnosti stiskanih palic iz zlitine CuAl10Ni5Fe4. Mikrostruktura je bila opazovana s svetlobnim in vrstičnim elektronskim mikroskopom. Preučevan je bil pojav in površinski delež faze α in κ ter njun vpliv na mehanske lastnosti. Z metodama DSC in EBSD je bila pregledana prisotnost trde in krhke γ_2-faze, ki poslabša korozijsko odpornost materiala. Rezultati so bili primerjani s podatki za močno legiran CuAl14Fe5 aluminijev bron, pri katerem ($\beta + \gamma_2$)-faza znižujeta veliko trdoto in odpornost proti obrabi.

Ključne besede: aluminijev bron, toplotna obdelava, mikrostruktura, mehanske lastnosti, DSC, EBSD, γ_2-faza

1 INTRODUCTION

CuAl10Ni5Fe4 aluminium bronze is a copper alloy that retains its high strength even at elevated temperatures and which possesses a good corrosion resistance and a high wear resistance.[1–3] It has a two-phase microstructure consisting of the poor-formability α phase and the high-temperature β phase, which exhibits excellent hot formability. The addition of nickel increases the alloy's strength without diminishing its excellent ductility, toughness and corrosion resistance. Typical applications of the alloy include valve seats, plunger tips, marine engine shafts, valve guides, aircraft components and pump shafts. The alloy exhibits limited cold formability (due to rapid work hardening), but excellent hot formability in the $\alpha + \beta$ region. The recommended forming temperatures are between 700 °C and 900 °C.[1,2]

Depending on the cooling rate and the subsequent heat treatment, the β phase may undergo a martensitic transformation into the unstable phase β', which, being very hard and brittle, enhances the strength and reduces the ductility of the material. In addition, other phases are found in the microstructure, which are termed κ, which consist mostly of Fe and Al or Ni,[3–5] or the γ_2 phase known to occur in Cu-Al binary alloys. The γ_2 phase in alloys containing less than 11.8 % aluminium forms during slow cooling or in the course of annealing at temperatures below 565 °C. These phases increase the strength and reduce the ductility of the alloy. The microstructure therefore consists of the α phase and the $\alpha + \kappa + \gamma_2$ eutectoid, as shown in the phase diagram in **Figure 1a**.[6]

Several types of the kappa phase have been classified: the sources[3–5,7,8] list four types, denoted as κ_I, κ_{II}, κ_{III}, κ_{IV}. The κ_I phase forms large dendrite-shape particles that are rich in Fe, which consist of Fe_3Al with Cu and Ni and the cubic structure DO_3. The phase κ_{II} forms smaller, globular particles with identical composition

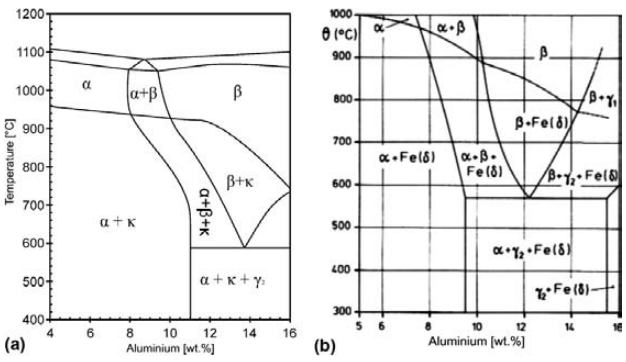

Figure 1: a) Vertical section of the phase diagram of nickel aluminum bronze with 5 % Ni and 5 % Fe, b) vertical section of phase diagram of Cu-Al-Fe at 3 % Fe

Slika 1: a) Navpični prerez faznega diagrama nikelj – aluminijev bron s 5 % Ni in 5 % Fe, b) navpični prerez faznega diagrama Cu-Al-Fe pri 3 % Fe

and structure to κ_I. The phase (precipitates) κ_{III} are NiAl-based and have the cubic B2 structure and a plate or lamellar shape. The κ_{IV} particles are small precipitates based on Fe_3Al. The composition of the γ_2 phase is Cu_9Al_4 and its structure is the cubic P-43m type.

Where tough requirements for hardness and wear resistance are to be met, high-alloyed Cu-Al-Fe aluminium bronzes are used with an aluminium level above 13 % and an iron content of up to 5 %. The microstructure of these alloys consists of two phases as well, as shown in the phase diagram in **Figure 1b**[9]: α and γ_2. The high hardness of these alloys is due to the latter, the γ_2 phase, which also exhibits a high hardness and brittleness, but a lower corrosion resistance. Owing to their hardness, excellent compressive strength and wear resistance, and sliding properties, these alloys are used for forming and drawing stainless steels and for worm wheels, valve guides and seats.

2 EXPERIMENTAL

Hot-pressed bars with a diameter of 32 mm from an alloy containing 10 % Al, 5 % Ni and 4 % Fe were used for the experiment. The material is denoted as CuAl10Ni5Fe4 (CW307G) according to EN 12163.

Specimens of bars were used for investigating the influence of annealing between 500 °C 30 min and 850 °C 30 min, quenching from 930 °C and aging of the quenched specimens at 30 °C 30 min to 400 °C 30 min upon the microstructure and mechanical properties. Attention was also paid to the influence of the slow cooling in the furnace and the subsequent rapid cooling after removal from the furnace. The results were compared with data for the high-alloyed CuAl14Fe5 aluminium bronze (sample of a worm wheel).

The chemical compositions of both alloys are given in **Table 1**.

The microstructures were observed on conventional metallographic sections in light (LM) and scanning electron microscopes (SEM). The HV hardness of the materials was measured. The evolution of the microstructure and the formation of the precipitates and phases were monitored using DSC (Differential Scanning Calorimetry) with a LINNSEIS DSC PT 1600 instrument and by means of EBSD (Electron Backscatter Diffraction) in a JEOL JSM 7400F scanning electron microscope equipped with a HKL-NORDLYSS camera and Channel5 software.

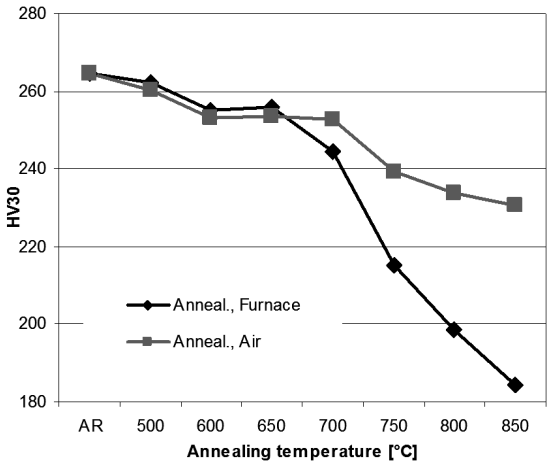

Figure 2: HV30 hardness of annealed specimens
Slika 2: Trdota HV30 vzorcev po žarjenju

Table 1: Chemical composition of alloys in mass fractions (*w*/%)
Tabela 1: Kemijska sestava zlitin v masnih deležih (*w*/%)

Alloy	Cu	Al	Ni	Fe	Mn	Sn	Si	Zn	Pb
CuAl10Ni5Fe4	balance	9.9	5.4	4.5	0.77	0.02	0.13	0.02	0.01
CuAl14Fe5	balance	14.5	0.12	4.9	0.97	0.06	0.22	0.006	0.07

3 RESULTS AND DISCUSSION

3.1 CuAl10Ni5Fe4 Alloy

3.1.1 HV Hardness

The HV30 hardness of the as-received specimens (AR) upon annealing was measured. The results are shown in **Figure 2**. The graph shows the hardness levels after annealing of the as-received material and upon annealing (tempering) of the quenched material. The hardness of the as-received material is 265 HV30. Quenching increases this value to 305, and aging, to 400 (**Table 2**).

Table 2: HV30 hardness
Tabela 2: Trdota HV30

Condition	Annealed	
cooling	Furnace	Air
AR	265	
500 °C	262	260
600 °C	255	253
650 °C	256	254
700 °C	245	253
750 °C	215	239
800 °C	198	234
850 °C	184	230
Quenched 930 °C 30 min		305
Quenched + Aged 400 °C 30 min		400

The hardness decreases during annealing; first slowly, while the temperature is below 700 °C, but more rapidly when it reaches 750 °C. A greater drop in hardness was seen in the specimens cooled slowly in a furnace than in those cooled in air.

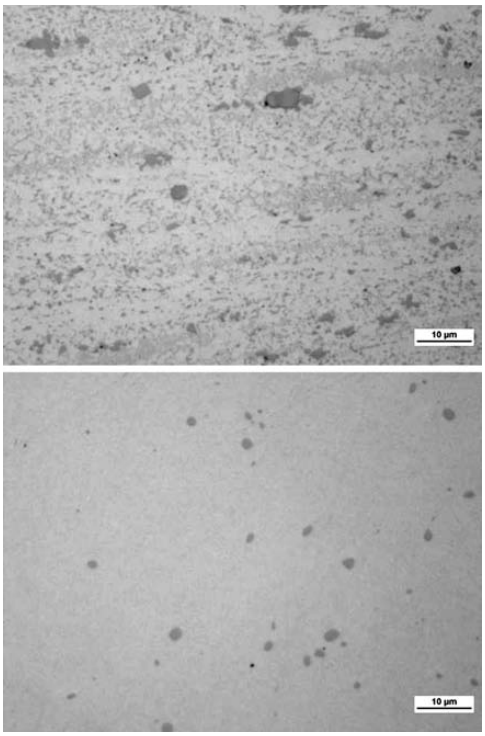

Figure 3: Micrographs of unetched specimens: a) as-received condition (AR), b) 17 – upon quenching

Slika 3: Mikrostruktura nejedkanih vzorcev: a) dobavljeno stanje (AR), b) 17 – po kaljenju

3.1.2 Microstructure

The micrographs of the specimens prior to etching are shown in **Figure 3**. Unetched sections show grey globular particles of the κ_{II} phase (according to EDS analysis, they contain 55 % iron, 11 % aluminium and nickel, copper, manganese and silicon), light grains of the phase α and a eutectoid consisting of $\alpha + \kappa$ or a balance of β. Annealing at the quenching temperature of 930 °C dissolves the κ phase in the eutectoid (except the globular κ_{II}) and the β phase transforms to the non-equilibrium β' phase,[10] as seen in **Figure 3b**.

The microstructures upon etching are shown in **Figures 4** and **5**. Etching reveals light grains of the phase α, grey to light-blue globular particles of the phase κ_{II} and the dark eutectoid $\alpha + \kappa_{III}$.[7] In the as-received state, the α grain size is very small: 1 µm to 2 µm. With increasing annealing temperature, the size of the α grains grows, as does the size of the eutectoid areas between them. Slow cooling in the furnace leads to coarsening of the κ precipitates and to the formation of larger amounts of lamellar κ_{III} precipitates in the eutectoid. The phase κ also precipitates along the α grain boundaries. With increasing α grain size the strength and hardness decrease. The greatest drop is seen in specimens annealed at 850 °C with slow cooling. However, the elongation decreases as well, which may be attributed to κ precipitating more frequently at the α grain boundaries.

Rapid cooling leads to a higher proportion of the eutectoid at the expense of the α proportion. In addition, a certain fraction of β phase is retained in the microstructure (more dark areas in the eutectoid). This is shown in **Figures 4c** and **4d**, where short etching with $NH_4OH+H_2O_2$ revealed an orange β phase, a bright α phase and the κ phase and eutectoid in light-blue colour.

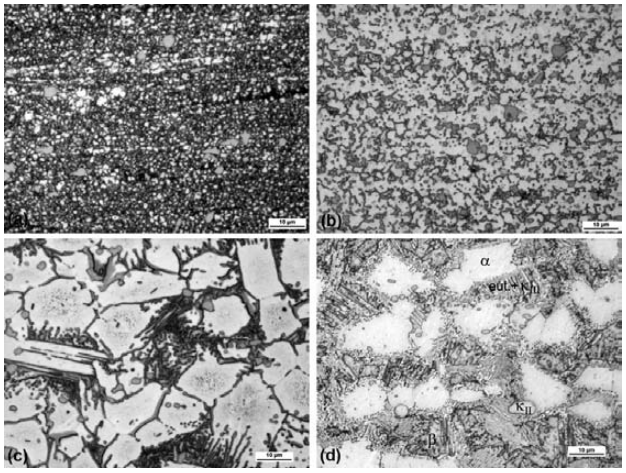

Figure 4: Micrographs of etched specimens: a) as-received condition, b) condition upon annealing at 750 °C, furnace, c) condition upon annealing at 850 °C, furnace, d) condition upon annealing at 850 °C, air

Slika 4: Mikrostruktura jedkanih vzorcev: a) dobavljeno stanje, b) po žarjenju na 750 °C, ohlajanje v peči, c) po žarjenju na 850 °C, ohlajanje v peči, d) po žarjenju na 850 °C, ohlajanje na zraku

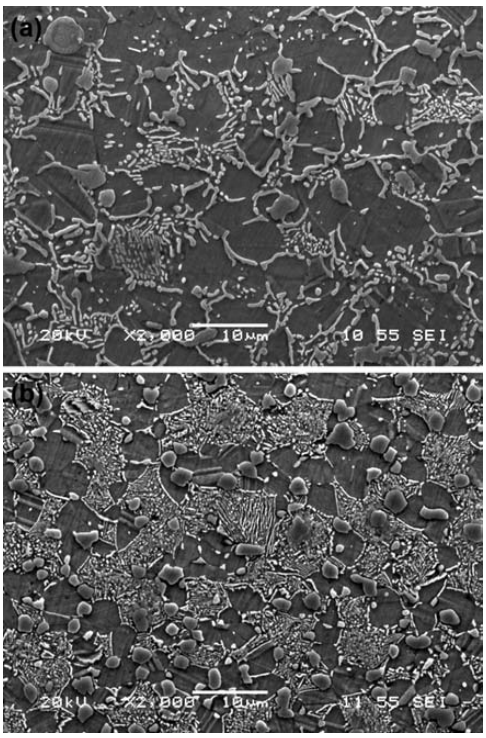

Figure 5: SEM micrographs of etched specimens: a) condition upon annealing at 800 °C, furnace, b) condition upon annealing at 800 °C, air

Slika 5: SEM-posnetka jedkanih vzorcev: a) po žarjenju na 800 °C, ohlajanje v peči, b) po žarjenju na 800 °C, ohlajanje na zraku

In contrast to the products of slow cooling, the κ precipitates are finer. Globular precipitates of κ_{IV} formed as well. The decrease in the strength and hardness is not as great as on slow cooling, which can be explained by a greater proportion of eutectoid and residual β in the microstructure.

The SEM micrographs also confirm that slow cooling leads to coarser κ precipitates than rapid cooling (**Figures 5a** and **5b**).

Upon quenching and aging, fine κ_{IV} precipitates form in the martensitic β' phase, as shown in the light (**Figure 6a**) and scanning electron (**Figure 6b**) micrographs. The martensitic β' phase and fine precipitates provide the quenched and aged material with high hardness.

3.2 CuAl14Fe5 Alloy

3.2.1 Hardness and microstructure

The specimen of CuAl14Fe5 alloy was made from a sample taken from a worm-wheel, in which very high hardness was required. The alloy corresponds to the AMPCO® 22 material by AMPCOMETAL.[11] According to the company information, it contains β and γ_2 phases and has a nominal hardness of 332 HB30.

The specimen was used for an annealing trial at 950 °C 30 min with subsequent cooling in air. The hardness of the as-received material was 422 HV10. During annealing, it rose to 462 HV10. Light micrographs are shown in **Figures 7a** and **7c**, and a scanning electron micrograph is shown in **Figure 7b**. The microstructure consists of light-blue grains of γ_2 embedded in bright β phase matrix, of large dark κ_{II} particles in the γ_2 phase and of minute κ_{IV} precipitates within the β phase. In the as-received specimen, the microhardness of the γ_2 phase is 573 HV0.05 and that of the β phase reaches 341 HV0.05. The presence of the β (β') phase can be deduced from the material's high hardness. Due to annealing, the proportion of the γ_2 phase increased and, as a result of its high hardness, so did the hardness of the

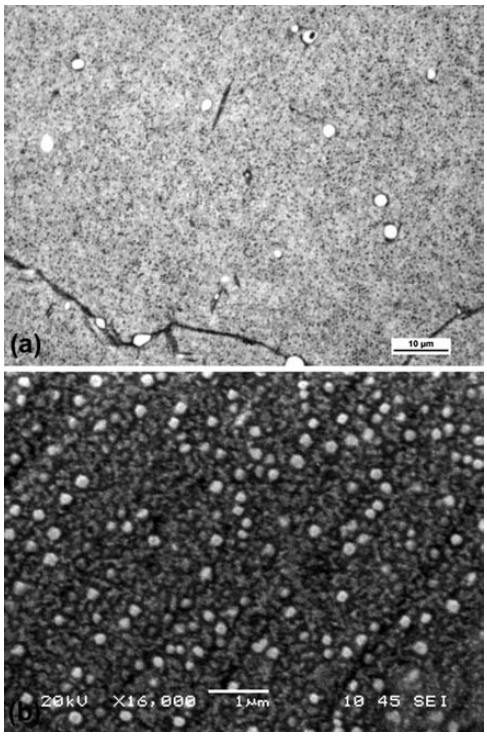

Figure 6: Microstructures of quenched and aged specimen, etched: a) quenched and aged at 400 °C (LM), b) quenched and aged at 400 °C (SEM)

Slika 6: Mikrostruktura hitro ohlajenega in staranega vzorca, jedkano: a) hitro ohlajeno in starano pri 400 °C (SM), b) hitro ohlajeno in starano pri 400 °C (SEM)

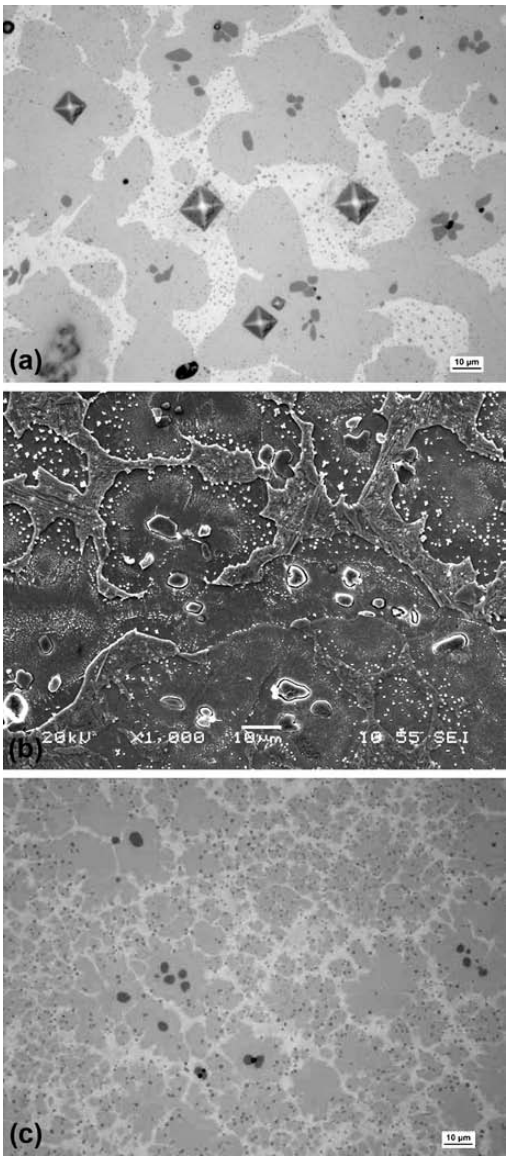

Figure 7: LM and SEM micrographs of CuAl14Fe5: a) as-received condition, unetched, HV0.05 hardness testing indentations (LM), b) as-received condition, etched (SEM), c) annealed at 950 °C 30 min, unetched (LM)

Slika 7: Svetlobni in SEM-posnetek CuAl14Fe5: a) dobavljeno stanje, nejedkano, odtiski trdote HV0,05 (SM), b) dobavljeno stanje, jedkano (SEM), c) žarjeno pri 950 °C 30 min, nejedkano (SM)

entire specimen. The SEM observation reveals needles of non-equilibrium β' phase in the β phase (**Figure 7b**).

3.3 DSC Analysis

Using DSC, the precipitation of the κ phases and the $\beta \rightarrow \alpha + \gamma_2$ eutectoid transformation were monitored.[12,13] DSC curves were measured at heating and cooling rates of 10 K/min. **Figure 8** shows the DSC curves for run 2 (after one cycle heating–cooling). The focus was the changes taking place at temperatures around 500 °C, in the vicinity of the eutectoid transformation $\beta \rightarrow \alpha+\gamma_2$ at 565 °C. Small peaks were recorded for the CuAl10Ni5Fe4 alloy. Temperature peaks between 930 °C and 830 °C on the cooling curve correspond to the formation of κ phases. ($\alpha+\beta \rightarrow \alpha+\beta+\kappa$) The peak at approx. 500 °C corresponding to the eutectoid transformation is very indistinct.

According to[7] at 930 °C the globular κ_{II} phase ($\beta \rightarrow \beta+\kappa_{II}$ transformation) precipitates from the β phase and at 800 °C the $\alpha+\kappa_{III}$ lamellar eutectoid forms ($\alpha \rightarrow \alpha+\kappa_{III}$). At 850 °C fine κ_{IV} precipitates form in the α phase.

In the CuAl14Fe5 alloy, the peaks due to the formation of the κ and γ_2 phases are much more pronounced. At temperatures below 800 °C, two peaks can be observed, which could indicate the formation of the κ and γ_2 phases in the β phase. The 500 °C peak may correspond to the $\beta \rightarrow \alpha + \gamma_2$ eutectoid transformation.

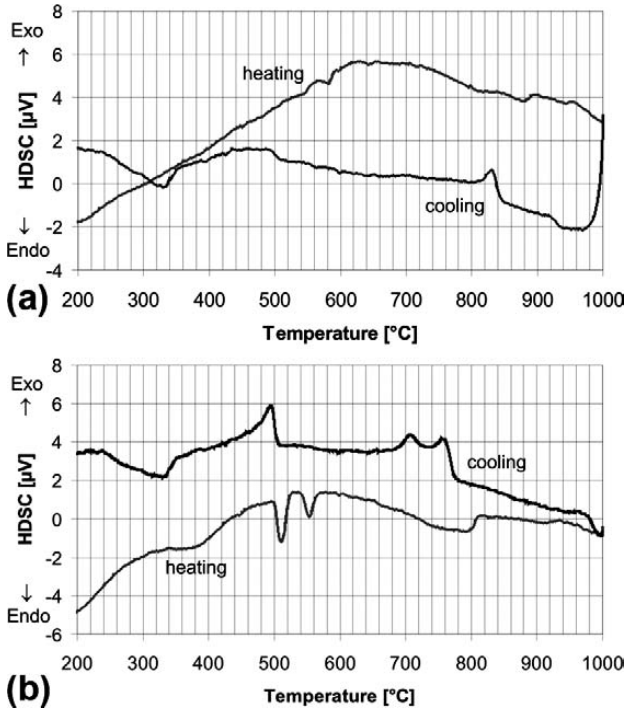

Figure 8: DSC curves for heating and cooling: a) CuAl10Ni5Fe4 alloy, b) CuAl14Fe5 alloy

Slika 8: DCS-krivulje pri ogrevanju in ohlajanju: a) zlitina CuAl10 Ni5Fe4, b) zlitina CuAl14Fe5

The transformation (formation of phases) at temperatures below 800 °C can be described according to **Figure 1b** as follows: $\beta \rightarrow \beta+\kappa \rightarrow \beta+\kappa+\gamma_2 \rightarrow \alpha+\kappa+\gamma_2$.

The peaks at temperatures of 300–400 °C correspond to the martensitic transformations of the β phase (formation of β_1, β').[10,13,14]

3.4 Identification of phases using EBSD

As the phases of the different structures produce different diffraction patterns (EBSP), the EBSD analysis can be used for identifying the various phases.[15] The EBSD analysis was aimed at identifying the κ and γ_2 phases in both aluminium bronzes. The phase maps and band contrast images are shown in **Figure 9**.

With the CuAl10Ni5Fe4 alloy, a higher band contrast was obtained (better quality of EBSP) in phases identified as α (large grey-coloured areas) and κ_{II} – Fe_3Al (small, bright spots). Due to the low band contrast, the phases in the eutectoid were not identified, most probably owing to the lamellar structure of $\alpha + \kappa_{III}$.

In the CuAl14Fe5 alloy, the phases identified included γ_2 (large grey areas) and κ_{II} (small bright spots). No regions with the β phase were identified, probably due to the presence of needles of non-equilibrium martensitic β' phase within the β phase.

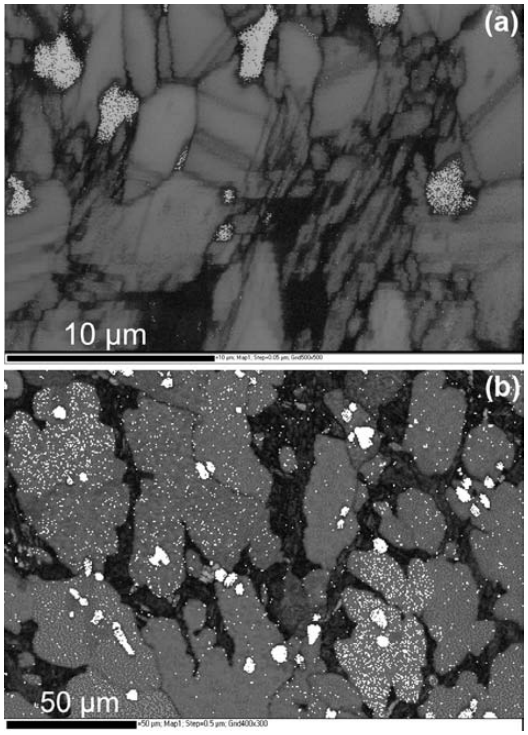

Figure 9: Band contrast and phase maps: a) alloy CuAl10Ni5Fe4, after annealing at 800 °C, air; grey phase – phase α, light phase – phase κ_{II}, b) alloy CuAl14Fe5, grey phase – phase γ_2, light phase – phase κ_{II}

Slika 9: Trakast kontrast in razporeditev faz: a) zlitina CuAl10Ni5Fe4 po žarjenju na 800 °C, ohlajeno na zraku; siva faza – faza α, svetla faza – faza κ_{II}, b) zlitina CuAl14Fe5, siva faza – faza γ_2, svetla faza – faza κ_{II}

4 CONCLUSIONS

The outcomes of the investigation of the effect of heat treatment on the microstructure and properties of pressed bars from CuAl10Ni5Fe4 alloy can be summarized as follows:

- Microstructure of the bars upon hot pressing is fine, consisting of α phase grains and the $\alpha + \kappa$ eutectoid. Owing to rapid cooling, the β phase may form as well.
- Annealing causes α grains and the eutectoid regions with κ_{III}-type precipitates to coarsen.
- Maximum hardness was obtained by quenching and aging at 400 °C: 400 HV30. This is due to the fine dispersion of particles κ in the martensitic β' phase.
- The γ_2 phase was not detected in the CuAl10Ni5Fe4 alloy by DSC or EBSD analysis.

CuAl10Ni5Fe4 Alloy

- The hardness of the CuAl14Fe5 is higher. It is determined by the proportion of the very hard γ_2 phase (with a microhardness of more than 550 HV0.05) in the β phase. The as-received specimen had a hardness of 422 HV10. Upon annealing, with subsequent air cooling, the fraction of γ_2 increased. The hardness increased as well: to a level of 462 HV10.
- The microstructure consists of β phases with a greater fraction of γ_2, particles of κ_{II} within the γ_2 phase and minute κ_{IV} dispersoids in the β phase.
- The presence of κ and γ_2 phases was confirmed by DSC and EBSD analyses.

Acknowledgement

The results presented in this paper were developed under the project "West-Bohemian Centre of Materials and Metallurgy" CZ.1.05/2.1.00/03.0077 co-funded from European Regional Development Fund.

5 REFERENCES

[1] ASM Handbook Volume 02: Properties and Selection: Nonferrous Alloys and Special-Purpose Materials, ASM International, 1990
[2] J. R. Davis, ASM Specialty Handbook: Copper and Copper Alloys, ASM International, 2001
[3] M. Cook, W. P. Fentiman, E. Davis, Observations on the Structure and Properties of Wrought Copper-Aluminum-Nickel-Iron Alloys, J. Inst. Met., 80 (**1951-52**), 419–429
[4] P. Brezina, Heat treatment of complex aluminum bronzes, International Metals Reviews, 27 (**1982**) 2, 77–120
[5] F. Hasan, A. Jahanafrooz, G. W. Lorimer, N. Rildley, The morphology, crystallography and chemistry of phases in as-cast nickel-aluminum bronze, Metallurgical Transactions A, 13 (**1982**), 1337–1345
[6] H. J. Meigh, Cast and Wrought Aluminum Bronzes – Properties, Processes and Structure, Institute of Materials, London, 2000
[7] E. A. Culpan, G. Rose, Microstructural characterization of cast nickel aluminium bronze, Journal of Materials Science, 13 (**1978**), 1647–1657
[8] A. Jahanafrooz, F. Hasan, G. W. Lorimer, N. Ridley, Microstructural Development in Complex Nickel-Aluminum Bronze, Met. Trans A., 14 (**1983**), 1951–1956
[9] CDA Publication, No 94, Equilibrium Diagrams, Selected copper alloy diagrams illustrating the major types of phase transformation, 1992
[10] R. K. Gupta, B. R. Ghosh, P. P. Sinha, Choice of heat treatment mode for increasing the hardness of Cu – 9% Al – 6% Ni – 5% Fe alloy, Metal Science and Heat Treatment, 47 (**2005**), 526–528
[11] AMPCO 22 Technical Data Sheet, http://www.ampcometal.com/common/datasheets/en/A22_EX_E.pdf, Accessed on 22 Oct. 2013
[12] B. P. Pisarek, Model of Cu-Al-Fe-Ni Bronze Crystallization, Archives of Foundry Engineering, 13 (**2013**) 3, 72–79
[13] M. Kaplan, A. K. Yildiz, The effects of production methods on the microstructures and mechanical properties of aluminum bronze, Materials Letters, 57 (**2003**), 4402–4411
[14] A. A. Hussein, Structure-Property Relationships in Dual-Phase Cu-Al Alloys: Part I. Individual Phases, Metall. Trans. A, 13 (**1982**), 837–846
[15] J. A. Schwartz, Electron Backscatter Diffraction in Materials Science, Kluwer Academic / Plenum Publishers, 2000